Journal of
Applied Crystallography
ISSN 0021-8898

Received 27 January 2009
Accepted 19 June 2009

Slow cooling of protein crystals

Matthew Warkentin and Robert E. Thorne*

Physics Department, Cornell University, Ithaca, NY 14853, USA. Correspondence e-mail: ret6@cornell.edu

Cryoprotectant-free thaumatin crystals have been cooled from 300 to 100 K at a rate of 0.1 K s^{-1} – 10^3–10^4 times slower than in conventional flash cooling – while continuously collecting X-ray diffraction data, so as to follow the evolution of protein lattice and solvent properties during cooling. Diffraction patterns show no evidence of crystalline ice at any temperature. This indicates that the lattice of protein molecules is itself an excellent cryoprotectant, and with sodium potassium tartrate incorporated from the 1.5 *M* mother liquor ice nucleation rates are at least as low as in a 70% glycerol solution. Crystal quality during slow cooling remains high, with an average mosaicity at 100 K of 0.2°. Most of the mosaicity increase occurs above ∼200 K, where the solvent is still liquid, and is concurrent with an anisotropic contraction of the unit cell. Near 180 K a crossover to solid-like solvent behavior occurs, and on further cooling there is no additional degradation of crystal order. The variation of *B* factor with temperature shows clear evidence of a protein dynamical transition near 210 K, and at lower temperatures the slope d*B*/d*T* is a factor of 3–6 smaller than has been reported for any other protein. These results establish the feasibility of fully temperature controlled studies of protein structure and dynamics between 300 and 100 K.

1. Introduction

X-ray crystallography performed on crystallized proteins is an essential tool in modern structural biology. The structural data obtained depend upon the temperature and thermal history of the protein crystal. Protein crystals are typically grown at temperatures (*T*) between 277 and 300 K, and then flash cooled to *T* = 100 K to reduce structural damage caused by the X-rays (Hope, 1988, 1990; Rodgers, 1994; Garman & Schneider, 1997; Garman, 1999; Pflugrath, 2004). The cooling process increases the amount of disorder within the crystal, most clearly manifested in large increases in mosaicity, and this reduces the quality of the information about molecular structure that can be obtained (Low *et al.*, 1966; Singh *et al.*, 1980).

Why and how cooling creates disorder in protein crystals are still not understood, but a growing body of work has addressed this problem (Walker *et al.*, 1998; Teng & Moffat, 1998; Snell *et al.*, 2002; McFerrin & Snell, 2002; Juers & Matthews, 2004*a*; Gakhar & Wiencek, 2005). Crystal order at *T* = 100 K has been examined using a variety of methods including X-ray crystallography and X-ray topography (Kriminski *et al.*, 2002; Lovelace *et al.*, 2006). Factors affecting this order including cryoprotectant type and concentration (Mitchell & Garman, 1994; Juers & Matthews, 2004*b*), flash-cooling protocol (Warkentin *et al.*, 2006), application of high pressures during cooling (Kim *et al.*, 2005), and post-cool crystal annealing (Harp *et al.*, 1998, 1999; Kriminski *et al.*, 2002) have been examined.

Although nearly all protein crystallography is performed at *T* = 100 K, X-ray data collection at higher temperatures – especially between the solvent glass transition temperature (∼150–180 K) and room or body temperature – can provide information about the protein's conformation, energy landscape and dynamics which is useful in understanding protein function. A few studies have examined how protein and crystal structure evolve with temperature, usually by flash cooling individual crystals from room temperature to different final temperatures (Frauenfelder *et al.*, 1979; Singh *et al.*, 1980; Chong *et al.*, 2001; Edayathumangalam & Luger, 2005). These studies have required large (∼50%) cryoprotectant concentrations to prevent crystalline ice formation below $T \simeq 270$ K, and these may have affected the protein structure and its temperature evolution. Changes within individual flash-cooled crystals upon warming from *T* = 100 K toward 200 K have also been explored (Weik *et al.*, 2001, 2005).

Collecting usable diffraction data near *T* = 200 K has proven particularly difficult (Frauenfelder *et al.*, 1979; Tilton *et al.*, 1992; Rasmussen *et al.*, 1992; Kurinov & Harrison, 1995). For example, Tilton *et al.* reported that at *T* = 200 K a ribonuclease A crystal rapidly became opaque and ceased to diffract, despite the use of 50%(*v*/*v*) 2-methyl-2,4-pentanediol (MPD). The only successes at this temperature used a methanol concentration of 75%(*v*/*v*) (Singh *et al.*, 1980), or crambin, an unusually small and dry protein crystal system (Teeter *et al.*, 2001).

The temperature-dependent properties of protein crystals depend upon both the protein and the solvent. The protein

molecules are fully (or nearly fully) hydrated, and their packing leaves solvent-filled channels and pockets that are typically 15–30 Å in size (and sometimes much larger). Protein crystals are thus protein–solvent composites, consisting of a regular lattice of protein molecules interwoven with a lattice of solvent-containing channels. The temperature-dependent properties of the protein, the solvent and their interaction must all be important in determining the temperature-dependent properties of protein crystals.

Here we extend previous work by measuring the evolution of the diffraction properties of a single protein crystal during cooling from 300 to 100 K. We demonstrate that crystals can be successfully cooled to 100 K without crystalline ice formation using cooling rates of $\sim$0.1 K s^{-1}, 10^3–10^4 times smaller than in previous studies, and even in the absence of penetrating cryoprotectants. Successful slow cooling requires careful removal of all external solvent, which otherwise will crystallize, generating intense ice diffraction rings that obscure protein crystal diffraction, drawing solvent out of the crystal (Weik *et al.*, 2001) and seeding ice crystal growth within the crystal that degrades crystalline order. Diffraction data can be collected continuously during cooling, so that the evolution of crystal, protein and solvent properties can be characterized as a function of temperature. Our method should be of particular use in probing conformation changes such as in 'kinetic crystallography', where enzymatic function is induced in the crystalline state and temperature variations can be used to trap reaction intermediates (Bourgeois & Royant, 2005; Colletier *et al.*, 2008; Bourgeois & Weik, 2009). The present data also provide insight into the protein glass/dynamical transition and into why crystal mosaicity increases during cooling.

2. Methods

Tetragonal crystals of thaumatin (MW = 24 000 Da, unit-cell dimensions $a = b = 58$, $c = 151$ Å, 56% solvent, 25–35 Å diameter solvent channels) were grown according to a standard recipe (McPherson, 1999). Protein from Sigma (product No. T 7638, lot No. 108FO299) was dissolved in 100 m*M* potassium phosphate buffer at pH 6.8 to a final concentration of 25 mg ml^{-1}. A well solution of 1.5 *M* sodium potassium tartrate was prepared in the same buffer. In each well of a 24-well plate, a glass cover slip with a hanging drop formed by mixing 5 µl of protein solution and 5 µl of well solution was suspended above 500 ml of well solution, and the well was sealed with vacuum grease.

For the cryoprotectant soaks, solutions with glycerol concentrations of 10, 20, 30 and 40%(*w*/*v*) were prepared by mixing glycerol and well solution. Crystals were serially soaked in solutions of increasing glycerol concentration until the desired final concentration was reached. The crystal was allowed to equilibrate at intermediate concentrations for $\sim$1 min and at the final concentration for between 5 and 10 min before further preparation.

Bulk solvent surrounding a crystal rapidly crystallizes during cooling through the T = 240–220 K temperature range and must be completely removed for successful slow cooling and X-ray data collection. Fig. 1 illustrates the method used to prepare crystals for slow cooling. Crystals were transferred from their mother liquor (the drop from which the crystal grew) or from a cryoprotectant soak to a large drop of Paratone-N oil (Hampton Research, Aliso Viejo, CA, USA) (Fig. 1*a*) or NVH oil (Cargille Laboratories, Cedar Grove, NJ, USA), using a MicroMount (Mitegen LLC, Ithaca, NY, USA) to minimize the transfer of excess mother liquor. The mixture was stirred so that the crystals shed their surrounding solvent in a trail of emulsified bubbles (Fig. 1*b*). The crystals were then transferred to a fresh oil drop and the process repeated until solvent trails were no longer visible. Pockets of solvent often remained stuck to the crystal surface (Fig. 1*c*) and were scraped off using a MicroChisel (Mitegen LLC, Ithaca, NY, USA).

When this process was properly executed, the facets of the crystal became nearly invisible (Fig. 1*d*). The change was unmistakable and did not depend upon illumination or magnification. We interpret this abrupt change in the appearance of the crystal as follows. The refractive index of the solvent varies between $\sim$1.33 (water) and $\sim$1.38 (40% glycerol); the refractive index of the crystal is likely near $n \simeq 1.56$ measured for tetragonal lysozyme (Cervelle *et al.*, 1974); and the refractive index for Paratone oil is likely near the n = 1.52 of NVH oil. If there is a layer of solvent coating the crystal, it creates two interfaces, oil–solvent and solvent–crystal, with large ($\Delta n \simeq 0.15$) refractive index steps. Since the reflection coefficient of an interface is proportional to the

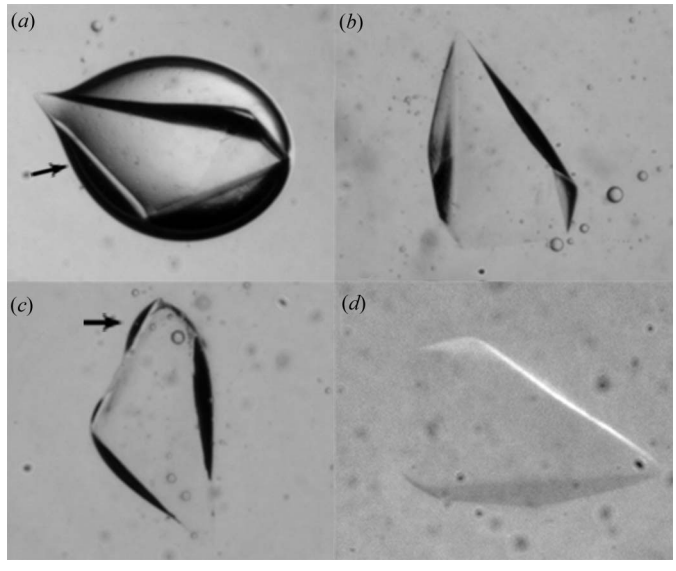

Figure 1
Preparation of a thaumatin crystal for slow cooling. (*a*) The crystal and surrounding mother liquor are transferred to a large drop of Paratone-N oil. (*b*) The crystal is stirred to remove most of the external mother liquor. (*c*) The remaining mother liquor, which tends to form beads (indicated by the arrow), is scraped off with a MicroChisel. (*d*) When all the external solvent has been removed, the crystal becomes nearly invisible in the oil, indicating that the solvent layer is no thicker than the wavelength of illuminating light. The actual solvent layer is likely to be much thinner, because any significant layer is unstable to beading on the surface.

refractive index difference, light incident from either the oil or the crystal is strongly reflected at both interfaces. When all the solvent has been removed (or at least when its remaining thickness is much smaller than the illuminating light wavelength, ~400 nm), the crystal is nearly index matched with the oil, little reflection occurs at the oil–crystal interface and the crystal becomes nearly invisible. This simple visual test thus provides a very sensitive probe of residual solvent.

A crystal thus prepared was captured together with a thick surrounding layer of Paratone-N oil (to prevent dehydration during the initial stages of the experiment) in a 500 µm–1 mm nylon CryoLoop (Hampton Research, Aliso Viejo, CA, USA) (Fig. 2). The sample was immediately placed on a goniometer head and a T = 300 K nitrogen gas stream produced by an Oxford Cryosystems 600 Series Cryostream was directed at it. The Cryostream was programmed to cool the sample at 0.1 K s^{-1}, and the X-ray data-collection software programmed to repeatedly collect five 1° oscillation frames over the same 5° wedge. A computer running *Cryopad* software (Oxford Cryosystems) and connected to the Cryostream controller logged the gas-stream temperature, so that the temperature for each X-ray frame could be obtained by matching time stamps in the frame file header and in the temperature log file. Cooling and data collection continued until the Cryostream temperature reached 100 K, 34 min after the start of cooling.

X-ray data were collected at beamline A1 of the Cornell High-Energy Synchrotron Source (CHESS) by a Quantum 210 detector (ADSC, Poway, CA, USA) running in binned mode using ADSC Quantum data-collection software. Each 5° wedge of data was independently analyzed using *DENZO* and *SCALEPACK* (Otwinowski & Minor, 1997) to determine unit-cell parameters, mosaicity and Wilson B factor. Corrections to calculated mosaicities to account for the finite beam divergence are small, whereby the beam divergence is estimated at 0.035° in the worst case; thus the smallest of our reported mosaicities, 0.075°, would deconvolve to 0.066°. The Wilson B factor was determined by a fit to the intensity *versus* resolution data in the output of *SCALEPACK*, with a low-resolution cutoff of 4 Å.

To verify that radiation damage did not significantly affect our results, the same X-ray dose was delivered as during cooling from T = 300 to 100 K, but with the temperature held fixed at 300 K. Radiation damage for a given dose is approximately 50−100 times larger at 300 K than at 100 K (Kmetko *et al.*, 2006), so that the radiation damage measured at 300 K sets an upper bound on the damage incurred during cooling experiments. The dose was measured using an ion chamber at the end of the collimator, which was calibrated at the beginning and end of the experiment. The delivered dose increased the unit-cell volume by 0.02%, the mosaicity by 0.04° and the B factor by 1.5 $Å^2$. These changes are small compared with those induced by cooling.

This control experiment for radiation damage also serves as a control for dehydration, since water's vapor pressure and the dehydration rate are largest at T = 300 K; they are insignificant at (and below) T = 250 K, where the vapor pressure is a factor of 35 smaller. Dehydration decreases the unit-cell volume and usually has little effect on mosaicity except at large dehydrations (Dobrianov *et al.*, 2001). No evidence of dehydration-induced cell-volume changes were observed in our control experiment, or for a sample held for 1 h at T = 300 K before irradiation. The thick (~500 µm) Paratone-N layer surrounding the crystal provides an excellent vapor barrier.

Several other approaches were explored before settling on the sample preparation protocol described above. Mother liquor surrounding the crystal can be removed by allowing it to evaporate slowly either in air or (for much slower removal) through a very thin layer of oil while the sample is observed under a microscope. Unlike with direct mechanical removal of the mother liquor, evaporation leaves behind non-volatile salts that can crystallize, producing diffraction that interferes with that from the protein. For protein crystals grown from high-salt mother liquors (*e.g.* ribonuclease A grown in 4 M sodium chloride), salt crystal diffraction is observed on cooling even when surrounding mother liquor is mechanically removed, possibly because cooling decreases the salt's solubility below the crystal's initial salt concentration.

The high-viscosity Paratone-N oil used to remove mother liquor from the crystal surface and prevent dehydration also helps prevent sample motion during data collection at higher temperatures. Thick layers of less viscous oils [*e.g.* mineral and perfluoro(poly)ether oils] can allow excessive motion and diffraction data that cannot be indexed. Even with Paratone-N oil, the first few high-temperature X-ray frames sometimes indicated large (~5°) crystal motions. Pausing for ~5 min after mounting, centering and rotating the sample to the intended data-collection angle before collecting frames minimized these motions.

Paratone-N oil has one significant disadvantage that was not recognized until after the bulk of our data collection was complete. As will be discussed later, when slowly cooled to $T \simeq$ 255 K, a small fraction of the oil forms a microcrystalline phase that produces two sharp diffraction rings at 4.46 and 3.96 Å. These rings can be avoided either by rapidly cooling to below $T \simeq 255$ K or by using NVH immersion oil, which is also highly viscous but does not crystallize at cooling rates of 0.1 K s^{-1} (data not shown).

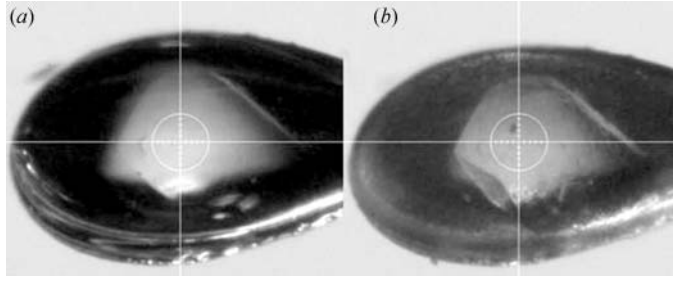

Figure 2
A thaumatin crystal prepared as in Fig. 1 and then mounted in a 1 mm CryoLoop with a large drop of oil, (*a*) at T = 300 K and (*b*) after slow cooling to T = 100 K. During slow cooling the surrounding oil becomes cloudy, indicating formation of a crystalline phase (see text). The thick oil layer prevents crystal dehydration.

Another approach to preventing dehydration during slow cooling is to enclose the sample together with a plug of mother liquor in MicroRT tubing (Mitegen, Ithaca, NY, USA) or in a glass X-ray capillary. Thick oil layers and associated crystal slippage can be eliminated. Using a liquid plug with a vapor pressure slightly lower than that of the mother liquor, the water surrounding the crystal can be evaporated without excessively dehydrating the crystal, eliminating the need for mechanical solvent removal. However, because the tubing/capillary length is comparable to or larger than the diameter of the Cryostream's gas stream, ice crystals tend to condense from the ambient air onto tubing outside the stream. Large temperature gradients across the tubing drive transport and condensation of water from the warmer liquid plug onto the colder sample, and this water eventually crystallizes. These difficulties can be overcome by expanding the cold gas stream or by shortening the tubing so that the tubing fits entirely within the constant-temperature portion of the stream.

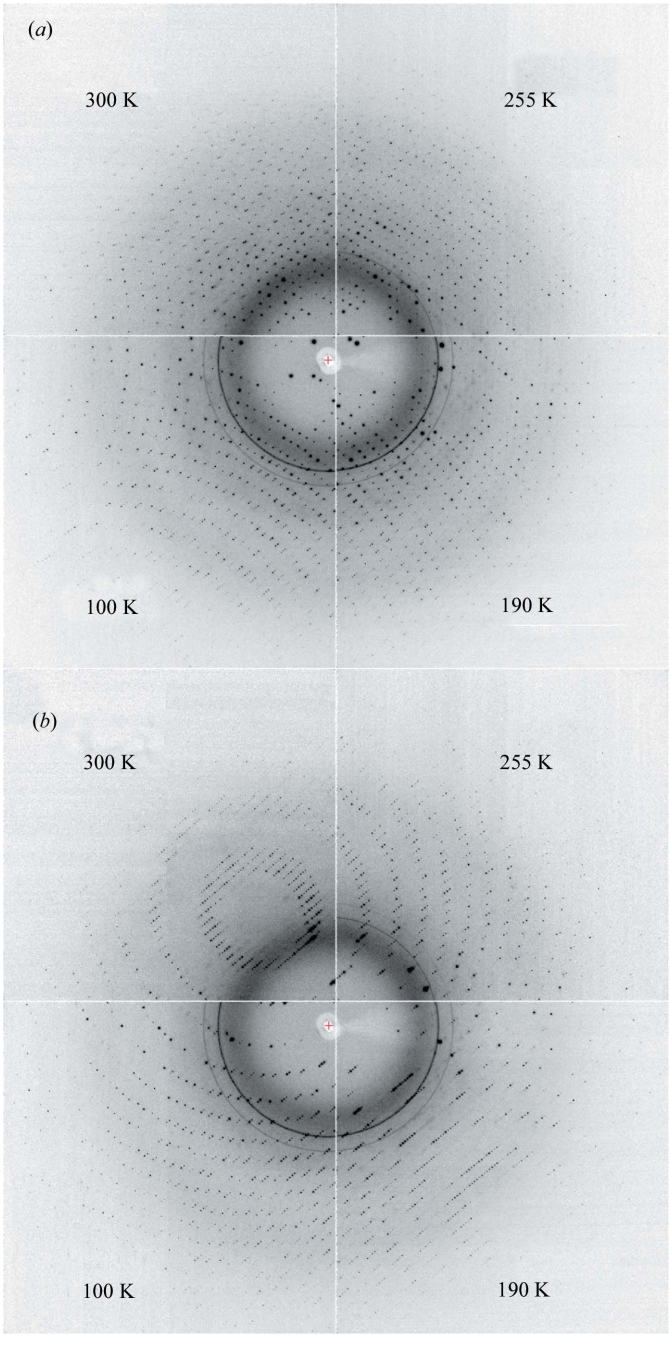

Figure 3
Diffraction images acquired at T = 300, 255, 190 and 100 K during slow cooling of (*a*) a thaumatin crystal prepared from its mother liquor and (*b*) a thaumatin crystal first soaked in 40%(*w*/*v*) glycerol/mother liquor solution. Although diffraction rings from the Paratone oil appear at 255 K, the crystal's diffraction quality does not visibly degrade and there is no evidence of ice during slow cooling.

3. Results

Thaumatin crystals survive slow cooling to T = 100 K, with or without a soak in 40% glycerol, and exhibit low-temperature diffraction properties that are comparable to or better than those of flash-cooled crystals. Fig. 3(*a*) shows diffraction patterns acquired from a single thaumatin crystal at four different temperatures as it was cooled. The crystal contained no cryoprotectants, and the only solutes present in the mother liquor were the buffer and 1.5 *M* sodium potassium tartrate. Fig. 3(*b*) shows diffraction patterns from a second slow-cooled thaumatin crystal differing only in that it was first soaked in mother liquor + 40%(*w*/*v*) glycerol.

Neither set of diffraction patterns shows any qualitative change on cooling, except that two sharp rings suddenly appear at $T \simeq 255$ K. These rings indicate that a crystalline phase has formed, but their positions do not correspond to those for ice. Their sudden appearance is not reflected in any change in the properties (unit cell, mosaicity, B factor) of the protein crystal, but coincides with a slight clouding of the oil surrounding the sample, visible at T = 100 K in Fig. 2(*b*). When a drop containing only Paratone-N oil is slow cooled, identical diffraction rings form at the same temperature, but no rings are observed when the drop is flash cooled. These results suggest that the rings are an artefact of slowly cooling the oil, and that the crystalline phase responsible does not interact with the protein crystal in any way.

Fig. 4 shows the unit-cell volume, mosaicity and Wilson B factor for two slow-cooled thaumatin crystals, one taken directly from the mother liquor and one soaked in a cryoprotectant solution. These quantities change most rapidly above $T \simeq 200$ K, and are more weakly temperature dependent below that temperature. At T = 100 K, the mosaicities are 0.15 and 0.20° for the as-grown and 40% glycerol samples, respectively. All of the mosaicity increase on cooling to T = 100 K occurs between T = 300 and ∼200 K; the mosaicity is constant below 200 K.

The B factor in Fig. 4(*c*) decreases on cooling, indicating a reduction in thermal motions. For the glycerol-free sample, there is an abrupt change in the slope dB/dT at $T \simeq 210$ K. Below $T \simeq 180$ K in both glycerol-free and glycerol-containing samples, the B factor varies linearly with temperature with a slope of 3×10^{-5} Å^2 K^{-1}. As discussed below, the slope change is a signature of the protein dynamical transition (glass transition) and the value of the slope below T = 180 K in

principle provides information about the protein's potential energy landscape.

The relative error (or random error) in each measurement is evident from the scatter in the points in Fig. 4. The absolute error (or systematic error) in the position of the whole curve is subject to a variety of sources of error, namely (i) the *B* factor that is obtained from *TRUNCATE* or *SCALEPACK* depends on the resolution range chosen and the model for the atomic form factor that is used and (ii) unit-cell volumes typically vary from crystal to crystal by 0.5%. These systematic errors are likely to be larger than the random errors.

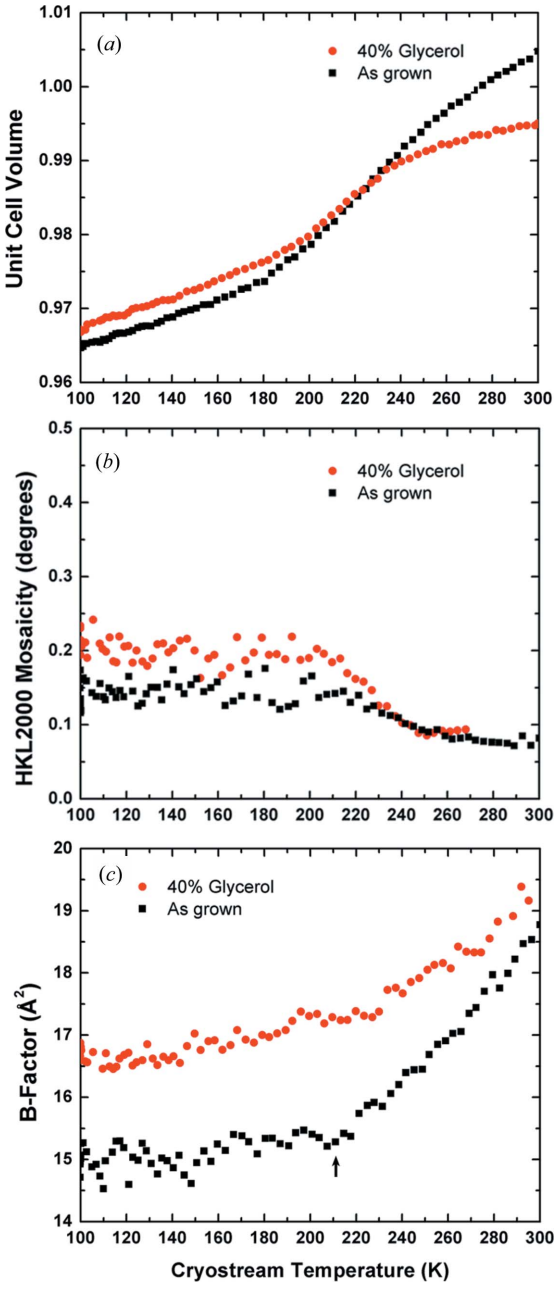

Figure 4
Relative cell volume, mosaicity and Wilson *B* factor of native and 40%(*w*/*v*) glycerol-soaked thaumatin crystals *versus* temperature during slow cooling. (*a*) The unit-cell volume for both samples rapidly contracts above ∼200 K, and contracts more modestly below 180 K. The contraction is anisotropic above 200 K but becomes isotropic below 180 K (see Fig. 6). The cell volume for both samples is referenced to an arbitrary value midway between their respective initial cell volumes. (*b*) The mosaicity increases most rapidly in the temperature range where the lattice contraction is both rapid and anisotropic. (*c*) The *B* factor decreases with decreasing temperature. The abrupt change in slope at ∼210 K (marked by an arrow) for the as-grown sample is evidence of a dynamical transition in the protein.

Fig. 5 shows how the diffuse X-ray background varies with temperature. The low-resolution diffuse intensity is clearly reduced at low temperatures. When this intensity is plotted *versus* temperature (data not shown), it also changes most rapidly above $T \simeq 200$ K, is relatively constant below that temperature and shows an abrupt change in slope near $T \simeq 210$ K. Arrows in Fig. 5 indicate the expected positions of Ih (hexagonal) and Ic (cubic) ice diffraction, but there is no evidence of either phase.

4. Discussion

4.1. Slow cooling gives high diffraction quality without penetrating cryoprotectants or high pressures

Slow cooling with no cryoprotectants – at rates 10^3–10^4 times slower than are achieved in flash cooling – yields thaumatin crystal mosaicities at $T = 100$ K that are as good as or better than have been obtained using any other method. The mosaicity of the as-grown (cryoprotectant-free) crystal in Fig. 3(*a*) increased from 0.08 to 0.15° on cooling to 100 K. Of the four slow-cooled thaumatin crystals examined (two at 0%

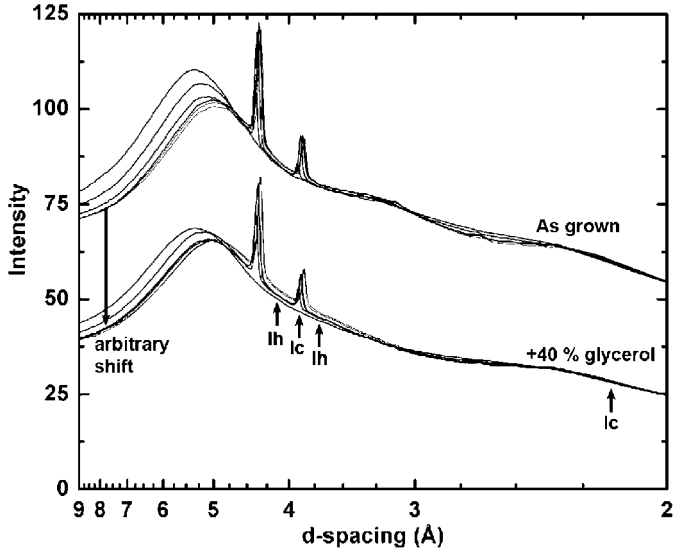

Figure 5
The azimuthally integrated X-ray background intensity *versus* resolution for the as-grown and 40%(*w*/*v*) glycerol thaumatin crystals, at temperatures (from top to bottom) of 300, 250, 210, 170, 140 and 100 K. The data for the glycerol-soaked crystal are shifted down by 25 for clarity. The large peak at 5.2 Å is diffuse scatter from the Paratone-N oil, and the sharp rings are due to a crystalline phase that forms within the oil during slow cooling. Arrows indicate the expected *d* values for Bragg scattering from ice, Ih or Ic. Most of the decrease in the diffuse scatter at low resolution on slow cooling occurs above $T = 200$ K, roughly tracking the behavior of the *B* factor in Fig. 4(*c*).

glycerol, one at 30% glycerol and one at 40% glycerol), the average $T = 100$ K mosaicity is 0.2°. This can be compared with a typical mosaicity of 0.4–0.5° for thaumatin crystals that have been flash cooled in our laboratory using conventional methods.

These results can also be compared with those of Kim *et al.* (2005), who examined penetrating cryoprotectant-free thaumatin crystals that were cooled under high pressures (up to 200 MPa) to prevent hexagonal ice formation. The average mosaicity for the four thaumatin crystals studied was 0.3°, and the smallest mosaicity obtained was 0.11°, much smaller than was obtained by Kim *et al.* using conventional flash cooling. The crystals were coated in NVH oil to prevent dehydration during pressurization – which removed external solvent – and the apparatus and cooling protocol gave relatively slow cooling rates (perhaps at 1–10 K s^{-1}). Our results show that high pressures were not needed to prevent ice crystallization within the crystals, and that the improved mosaicities may have been primarily due to external solvent removal by the oil, suppression of ice formation by the protein and slower cooling. High pressures may then only be necessary for crystals with very high solvent contents and large solvent channels (at least larger than the ∼35 Å in thaumatin), where the protein alone may provide inadequate cryoprotection.

4.2. How much ice is present in slow-cooled crystals?

The diffraction data in Fig. 5 show no evidence of the ice rings expected from either Ih or Ic ice, the two phases that can form at ambient pressure. As discussed above, the two observed peaks/rings are not due to ice, and are present when drops containing only Paratone-N oil are cooled. However, the smaller of the two oil-related peaks lies very close to the expected position of the low-resolution peak from ice Ic, and so could obscure the presence of a small amount of that ice phase.

The presence of ice Ic could be revealed in at least two ways. First, Ic has a strong second-order peak at 2.19 Å with an intensity 0.41 times that of the primary peak. No peak is observed at this position (indicated by an arrow) in Fig. 5. Second, the abrupt formation of cubic ice at some temperature should abruptly change the intensity ratio between the large and small Paratone-N peaks. No such change is observed.

An upper bound on the ice fraction present within our samples can be estimated as follows. The total number of scattered X-rays (into all of k space) from a given crystalline phase is proportional to the total integrated electron density in that phase that is illuminated (in real space) by the X-ray beam. Provided that a representative region of k space is examined, the ratio of the diffraction intensity from the two phases is equal to the ratio of the number of electrons in each phase. For our estimate, we include all diffraction data collected in a series of five 1° oscillation frames to a resolution of 1.8 Å, which include the positions of all integrable reflections from the protein and the first three rings from cubic ice. The total number of detected X-ray photons contained in the protein peaks is computed for each frame (as the sum of integrated peak intensities from *DENZO*) and varies by roughly 10% between frames. This total, averaged over five frames, is $\sim 2 \times 10^6$ 'intensity units' (as reported in the dark-corrected image file produced by the ADSC Q-210 detector software). This total is then used as an estimate of the total number of the illuminated electrons that are associated with the protein (in arbitrary units). Any disorder in the protein or its lattice shifts intensity from the peaks to the diffuse background, and so this is an underestimate.

Fig. 5 shows the X-ray intensity measured in a given resolution shell (one pixel wide), averaged over five frames/5° in φ (sample rotation), *versus* resolution. Pixels within a 10×10 pixel square centered on the position of each reflection (obtained from *DENZO*'s *.x* output files) were omitted from the average. A smooth fit to the background gives an estimate of the fluctuations (from all sources) in this averaged value of 0.1 'intensity units' per pixel. The ice Ic detection limit is proportional to this fluctuation level. It is inversely proportional to the grain size of the cubic ice, which determines the number of pixels over which ice diffraction is spread and thus the ice intensity in each pixel.

Consider the as-grown thaumatin sample. Using the Scherrer equation, the width of the powder ring (on the detector, in pixels) expected from microcrystallites of a given size can be calculated. If cubic ice with a grain size of 15 nm is present, then its first- and second-order reflections will illuminate approximately 10^5 pixels on the detector, including those pixels within each powder ring's FWHM. If detecting the ice requires an extra 0.1 'intensity units' in each of these pixels, then $\sim 10^4$ intensity units must be scattered from cubic ice to be detectable. The total integrated intensity per frame from protein for this sample was $\sim 10^6$, giving an order of magnitude upper bound for the ice fraction of less than 1%. If the ice instead has a grain size of 150 nm, then the detection limit according to this crude estimate would be 0.1%.

4.3. Why can crystals be slow cooled without cryoprotectants?

Key to the successful slow cooling of thaumatin crystals is the surprising fact that no ice forms within them, even when no penetrating cryoprotectants are used. Previous measurements on aqueous glycerol solutions (Sutton, 1991; Berejnov *et al.*, 2006; Warkentin *et al.*, 2008) have shown that glycerol concentrations of at least 50–60%(*w*/*v*) are required to prevent ice formation at cooling rates of 1 K s^{-1}. Extrapolating to the present cooling rate of 0.1 K s^{-1} implies that the protein and salt (derived from the 1.5 *M* sodium potassium tartrate of the mother liquor within thaumatin crystals) is as effective in inhibiting ice formation as 70%(*w*/*v*) glycerol. Sartor *et al.* (1995) have determined the minimum cooling rates needed to prevent ice formation in hydrated protein powders. For hydration levels of 0.56–0.73 (mass water/mass protein), the required cooling rates were 25–4 K s^{-1}. The hydration level in thaumatin (1.22) is much larger, and the required cooling rate is much smaller. This suggests that

regular crystalline packing of the protein increases its ability to inhibit ice nucleation.

Experiments on pure water in porous glass found that crystalline ice only forms in pores larger than ~25 Å (Rault *et al.*, 2003). In experiments on protein crystals, crystalline ice formed from vitrified solvent on warming from 150 to 200 K in crystals with solvent channels of 65 Å or larger, but no internal ice formed in crystals with solvent channels smaller than 20 Å (Weik *et al.*, 2001, 2005). Because the first hydration layer behaves very differently from bulk water, a protein crystal's effective pore/channel size for nucleation is reduced from its geometric value. Thus, the channel diameter of thaumatin crystals (25–35 Å) may be smaller than is required for nucleation of cubic ice on our experimental timescales.

4.4. Origins of disorder on cooling

The mechanisms that create disorder on cooling should be affected by cooling rate. Slower cooling allows more time for ice crystal nucleation and growth (and perhaps other processes) that degrade protein crystal diffraction properties, and this has been the most important obstacle in previous diffraction studies of slow-cooled crystals. On the other hand, slower cooling reduces thermal gradients within the crystal and associated crystal strains that can drive cracking and broaden mosaicity (Kriminski *et al.*, 2003).

Slower cooling may also reduce strains and disorder associated with the inherent thermal expansivity mismatch between the protein lattice and the solvent that fills its voids (Juers & Matthews, 2001, 2004*b*; Kriminski *et al.*, 2002; Lovelace *et al.*, 2006). This mismatch requires that the solvent either flows (to the crystal surface or to grain boundaries and other defective regions where the lattice is weak) or compresses. We estimate that pressures of 10–100 MPa could be generated within the crystal if negligible flow occurs, based upon the observed expansivity of the thaumatin lattice and the measured expansivity of water confined to 2 nm pores (Mallamace *et al.*, 2007). Slower cooling allows more time before vitrification for solvent to flow and to accommodate the contracting protein lattice, and so may reduce stresses and solvent pooling in defective regions and thereby help maintain crystal order.

In the present experiments, essentially all of the mosaicity increase occurs above 200 K, where the mismatch between solvent expansion and lattice contraction is large (Mallamace *et al.*, 2007). The largest rate of mosaicity increase occurs at temperatures (200–220 K) where the unit-cell volume is rapidly decreasing and the solvent viscosity is rapidly increasing. If expansion mismatch in fact accounts for some of the increased crystal disorder, one might expect that adding glycerol, which unlike water only contracts on cooling, would reduce the mismatch and the amount of disorder. However, glycerol also strongly increases solvent viscosity and reduces solvent diffusion, and so the flow required to relieve the stresses caused by any remaining mismatch is inhibited.

We also note that, above 200 K, thaumatin's lattice contraction on cooling is strongly anisotropic. Below 180 K it is very nearly isotropic (Fig. 6), and occurs at a rate ($\sim 10^{-4}$ K^{-1}) very close to the thermal contraction of amorphous water (also $\sim 10^{-4}$ K^{-1}) at that temperature (Mallamace *et al.*, 2007). Anisotropic contraction requires transport of solvent within the unit cell, *i.e.* solvent molecules must flow past or around protein molecules. Below 200 K, solvent flow and translational diffusion are negligible (Weik *et al.*, 2004; Wood *et al.*, 2007, 2008) and so contraction should become nearly isotropic.

4.5. Comparison with previous work

Petsko and co-workers demonstrated that ribonuclease A goes through a 'dynamical transition' at ~220 K (Tilton *et al.*, 1992; Rasmussen *et al.*, 1992). This transition was characterized by a kink in the crystallographic Debye–Waller factor (*B* factor), indicating the onset of long-range anharmonic motions (*e.g.* translational diffusion in the solvent, motion of surface side chains or larger conformational changes) on warming above the transition temperature. This kink was also observed in mean square displacements measured in earlier Mössbauer spectroscopy studies of ^{57}Fe in myoglobin (Parak *et al.*, 1982), as well as with inelastic neutron scattering (Doster *et al.*, 1989), but the transition does not appear in myoglobin's crystallographic *B* factors (Chong *et al.*, 2001).

Fig. 4(*c*) shows the Wilson *B* factors of two slow-cooled thaumatin crystals. The crystal without glycerol shows a well defined kink (change in slope) in $B(T)$ signalling a transition at 210 K, whereas the crystal soaked in 40% glycerol shows what could be interpreted as a broadened transition. The integrated diffuse background intensity in the resolution range 15–5 Å, shown in Fig. 5, also shows a kink. This is not surprising, as both the *B* factor and diffuse scatter are related to thermal motions (and/or static disorder) of the protein. However, for both crystals the transition as seen through diffuse scatter occurs at a lower temperature than as seen through the *B* factor (associated with Bragg reflections). We note that this loss of diffuse intensity at low resolution cannot

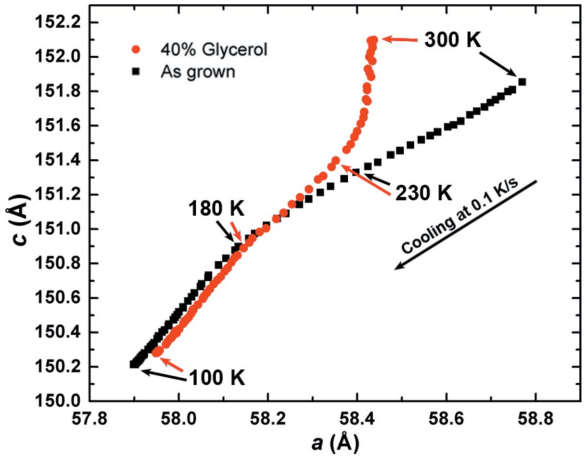

Figure 6
Lattice parameters *a versus c* during cooling for the as-grown and 40% glycerol crystals. Both crystals show very nearly isotropic contraction below ~180 K (indicated by an arrow).

be accounted for by the appearance of oil rings at $T = 255$ K: the diffuse intensity shows most of its decrease above 255 K, and it varies smoothly near 255 K despite the abrupt appearance of the oil rings.

Previous studies on flash-cooled protein crystals have shown that the solvent undergoes an amorphous solid-to-liquid transition as the temperature is increased through the range 180–220 K, driving a solid-like to liquid-like transition in the protein molecule itself. (Vitkup *et al.*, 2000; Weik *et al.*, 2001, 2005; Wood *et al.*, 2007, 2008). Below this transition, the B factor decreases linearly with decreasing temperature. This decrease is usually attributed to a reduction in the amplitudes of harmonic thermal motions, consistent with the notion that the system is solid-like below 180 K.

For slow-cooled thaumatin crystals (Fig. 4*c*), the average mean squared displacement's (MSD = $B/8\pi^2$) variation with temperature below $T = 180$ K is $\mathrm{dMSD}/\mathrm{d}T \simeq 5 \times 10^{-5}$ Å^2 K^{-1}. The dMSD/dT values obtained from crystals of myoglobin (Parak *et al.*, 1982; Chong *et al.*, 2001), ribonuclease A (Tilton *et al.*, 1992; Rasmussen *et al.*, 1992), lysozyme (Joti *et al.*, 2002), maltose binding protein (Wood *et al.*, 2008) and purple membrane (Wood *et al.*, 2007) are in the range 10^{-4}–10^{-3} Å^2 K^{-1}; the rate for hexagonal ice is $\sim 2 \times 10^{-4}$ Å^2 K^{-1} (Teeter *et al.*, 2001). These studies followed a variety of thermal trajectories from room temperature to the measurement temperature, including slow cooling and warming to each temperature (Parak *et al.*, 1982; Wood *et al.*, 2007, 2008), quenching from room temperature to each measurement temperature (Tilton *et al.*, 1992; Rasmussen *et al.*, 1992; Chong *et al.*, 2001; Teeter *et al.*, 2001), and quenching to low temperature and then slowly warming to each measurement temperature (Joti *et al.*, 2002). If the entire change in B is due to changes in harmonic motions, then thaumatin must be an unusually 'stiff' protein in this temperature range. $B(T)$ can also be affected by changes in static disorder. A reduced magnitude of dB/dT could result if there is a gradual increase in static disorder – either due to a gradual trapping of metastable microstates, or due to an increase in lattice-level disorder – during slow cooling.

Previous temperature-dependent studies of protein crystals required the use of large cryoprotectant concentrations. To prevent ice formation and loss of diffraction at temperatures approaching 200 K, Singh *et al.* (1980) used 45–75% methanol in their bovine trypsinogen crystals [47%(*w*/*v*) solvent]. Tilton *et al.* (1992) used 50% methanol or 50% MPD in their ribonuclease A crystals, but were still unable to obtain data at 200 K because the crystals 'rapidly became opaque and ceased to diffract'. These results highlight how remarkable it is that thaumatin can be successfully cooled to any temperature without cryoprotectants.

4.6. A generally applicable method?

The method described here has been applied to ribonuclease A (cell volume 225 000 Å^3, solvent content 45%), lysozyme (cell volume 220 000 Å^3, solvent content 36%), trypsin (cell volume 200 000 Å^3, solvent content 42%), insulin (cell volume 456 000 Å^3, solvent content 63%) and urease (cell volume 4 900 000 Å^3, solvent content 48%) crystals (Jabri *et al.*, 1992, 1995; Jabri & Karplus, 1996), in addition to the thaumatin samples described above. As-grown (cryoprotectant-free) urease and insulin crystals can be slow cooled to $T =$ 100 K without ice formation or significant degradation of diffraction quality, with a success rate of ∼75%, based upon approximately 15 trials. Lysozyme and trypsin crystals can be successfully slow cooled in 40% glycerol. However, when as-grown (cryoprotectant-free) crystals are cooled, diffraction quality abruptly degrades and cubic ice forms near $T = 210$ K, and in almost every case the diffraction is too poor to continue the experiment. Ribonuclease A crystals were grown in high salt (4 *M* sodium chloride), and this salt precipitated out as the temperature was lowered, destroying the crystalline order. These results suggest that, with continued methodological refinement, it may be possible to slow cool a substantial fraction of protein and virus crystals without the use of penetrating cryoprotectants. Slow cooling may thus provide an alternative as well as a complement to flash cooling in cryocrystallographic studies.

We have also successfully flash cooled thaumatin, lysozyme, trypsin, insulin and urease crystals to specific temperatures between 300 and 100 K using the same solvent-removal and -mounting protocol as for slow cooling and then simply placing them in a gas stream at the desired temperature. Although glycerol improves the success rate significantly, high-quality diffraction data have been obtained without the use of penetrating cryoprotectants from all five proteins.

5. Conclusion

The present results demonstrate that high-quality diffraction data can be continuously collected from an individual crystal, over the entire temperature range between 300 and 100 K, by cooling at 0.1 K s^{-1}. Successful slow cooling does not require large cryoprotectant concentrations or special apparatus (*e.g.* for generating high pressures), but only that all external solvent be removed from the crystal. Thaumatin crystals cooled in this way show exceptionally low mosaicity and no evidence of crystalline ice at $T = 100$ K. The small observed mosaicity increase occurs above 200 K, where the mismatch between protein lattice contraction and solvent expansion is largest and where the unit-cell contraction is anisotropic. This suggests that the mismatch is an important source of crystal disorder, as has been observed in previous studies.

Cooling rates 10^3–10^4 times slower than in conventional flash cooling (and 10^5–10^6 times slower than in hyperquenching; Warkentin *et al.*, 2006) will affect how a protein explores its energy landscape and the conformational states observed during and after cooling to low or intermediate temperatures. Slow cooling may thus provide a new window into protein structure and function.

This work was supported by the National Institutes of Health (NIH) under award No. GM065981-05A1. This work is

based upon research conducted at the Cornell High-Energy Synchrotron Source (CHESS), which is supported by the National Science Foundation (NSF) and the NIH/National Institute of General Medical Sciences under NSF award No. DMR-0225180, using the Macromolecular Diffraction at CHESS (MacCHESS) facility, which is supported by award No. RR-01646 from the NIH, through its National Center for Research Resources.

References

Berejnov, V., Husseini, N. S., Alsaied, O. A. & Thorne, R. E. (2006). *J. Appl. Cryst.* **39**, 244–251.
Bourgeois, D. & Royant, A. (2005). *Curr. Opin. Struct. Biol.* **15**, 538–547.
Bourgeois, D. & Weik, M. (2009). *Crystallogr. Rev.* **15**, 87–118.
Cervelle, B., Cesbron, F., Berthou, J. & Jolles, P. (1974). *Acta Cryst.* A**30**, 645–648.
Chong, S. H., Joti, Y., Kidera, A., Go, N., Ostermann, A., Gassmann, A. & Parak, F. (2001). *Eur. Biophys. J. Biophys. Lett.* **30**, 319–329.
Colletier, J. P., Bourgeois, D., Sanson, B., Fournier, D., Sussman, J. L., Silman, I. & Weik, M. (2008). *Proc. Natl Acad. Sci. USA*, **105**, 11742–11747.
Dobrianov, I., Kriminski, S., Caylor, C. L., Lemay, S. G., Kimmer, C., Kisselev, A., Finkelstein, K. D. & Thorne, R. E. (2001). *Acta Cryst.* D**57**, 61–68.
Doster, W., Cusack, S. & Petry, W. (1989). *Nature* (*London*), **337**, 754–756.
Edayathumangalam, R. S. & Luger, K. (2005). *Acta Cryst.* D**61**, 891–898.
Frauenfelder, H., Petsko, G. A. & Tsernoglou, D. (1979). *Nature* (*London*), **280**, 558–563.
Gakhar, L. & Wiencek, J. M. (2005). *J. Appl. Cryst.* **38**, 945–950.
Garman, E. (1999). *Acta Cryst.* D**55**, 1641–1653.
Garman, E. F. & Schneider, T. R. (1997). *J. Appl. Cryst.* **30**, 211–237.
Harp, J. M., Hanson, B. L., Timm, D. E. & Bunick, G. J. (1999). *Acta Cryst.* D**55**, 1329–1334.
Harp, J. M., Timm, D. E. & Bunick, G. J. (1998). *Acta Cryst.* D**54**, 622–628.
Hope, H. (1988). *Acta Cryst.* B**44**, 22–26.
Hope, H. (1990). *Annu. Rev. Biophys. Biophys. Chem.* **19**, 107–126.
Jabri, E., Carr, M. B., Hausinger, R. P. & Karplus, P. A. (1995). *Science*, **268**, 998–1004.
Jabri, E. & Karplus, P. A. (1996). *Biochemistry*, **35**, 10616–10626.
Jabri, E., Lee, M. H., Hausinger, R. P. & Karplus, P. A. (1992). *J. Mol. Biol.* **227**, 934–937.
Joti, Y., Nakasako, M., Kidera, A. & Go, N. (2002). *Acta Cryst.* D**58**, 1421–1432.
Juers, D. H. & Matthews, B. W. (2001). *J. Mol. Biol.* **311**, 851–862.
Juers, D. H. & Matthews, B. W. (2004*a*). *Q. Rev. Biophys.* **37**, 105–119.
Juers, D. H. & Matthews, B. W. (2004*b*). *Acta Cryst.* D**60**, 412–421.
Kim, C. U., Kapfer, R. & Gruner, S. M. (2005). *Acta Cryst.* D**61**, 881–890.
Kmetko, J., Husseini, N. S., Naides, M., Kalinin, Y. & Thorne, R. E. (2006). *Acta Cryst.* D**62**, 1030–1038.
Kriminski, S., Caylor, C. L., Nonato, M. C., Finkelstein, K. D. & Thorne, R. E. (2002). *Acta Cryst.* D**58**, 459–471.
Kriminski, S., Kazmierczak, M. & Thorne, R. E. (2003). *Acta Cryst.* D**59**, 697–708.
Kurinov, I. V. & Harrison, R. W. (1995). *Acta Cryst.* D**51**, 98–109.
Lovelace, J. J., Murphy, C. R., Pahl, R., Brister, K. & Borgstahl, G. E. O. (2006). *J. Appl. Cryst.* **39**, 425–432.
Low, B. W., Chen, C. C. H., Berger, J. E., Singman, L. & Pletcher, J. F. (1966). *Proc. Natl Acad. Sci. USA*, **56**, 1746–1750.
Mallamace, F., Branca, C., Broccio, M., Corsaro, C., Mou, C. Y. & Chen, S. H. (2007). *Proc. Natl Acad. Sci. USA*, **104**, 18387–18391.
McFerrin, M. B. & Snell, E. H. (2002). *J. Appl. Cryst.* **35**, 538–545.
McPherson, A. (1999). *Crystallization of Biological Macromolecules*. New York: Cold Spring Harbor Laboratory Press.
Mitchell, E. P. & Garman, E. F. (1994). *J. Appl. Cryst.* **27**, 1070–1074.
Otwinowski, Z. & Minor, W. (1997). *Methods in Enzymology*, Vol. 276, *Macromolecular Crystallography*, Part A, edited by C. W. Carter Jr & R. M. Sweet, pp. 307–326. New York: Academic Press.
Parak, F., Knapp, E. W. & Kucheida, D. (1982). *J. Mol. Biol.* **161**, 177–194.
Pflugrath, J. W. (2004). *Methods*, **34**, 415–423.
Rasmussen, B. F., Stock, A. M., Ringe, D. & Petsko, G. A. (1992). *Nature* (*London*), **357**, 423–424.
Rault, J., Neffati, R. & Judeinstein, P. (2003). *Eur. Phys. J. B*, **36**, 627–637.
Rodgers, D. W. (1994). *Structure*, **2**, 1135–1140.
Sartor, G., Hallbrucker, A. & Mayer, E. (1995). *Biophys. J.* **69**, 2679–2694.
Singh, T. P., Bode, W. & Huber, R. (1980). *Acta Cryst.* B**36**, 621–627.
Snell, E. H., Judge, R. A., Larson, M. & van der Woerd, M. J. (2002). *J. Synchrotron Rad.* **9**, 361–367.
Sutton, R. L. (1991). *J. Chem. Soc. Faraday Trans.* **87**, 101–105.
Teeter, M. M., Yamano, A., Stec, B. & Mohanty, U. (2001). *Proc. Natl Acad. Sci. USA*, **98**, 11242–11247.
Teng, T.-Y. & Moffat, K. (1998). *J. Appl. Cryst.* **31**, 252–257.
Tilton, R. F., Dewan, J. C. & Petsko, G. A. (1992). *Biochemistry*, **31**, 2469–2481.
Vitkup, D., Ringe, D., Petsko, G. A. & Karplus, M. (2000). *Nat. Struct. Biol.* **7**, 34–38.
Walker, L. J., Moreno, P. O. & Hope, H. (1998). *J. Appl. Cryst.* **31**, 954–956.
Warkentin, M., Berejnov, V., Husseini, N. S. & Thorne, R. E. (2006). *J. Appl. Cryst.* **39**, 805–811.
Warkentin, M., Stanislavskaia, V., Hammes, K. & Thorne, R. E. (2008). *J. Appl. Cryst.* **41**, 791–797.
Weik, M., Kryger, G., Schreurs, A. M. M., Bouma, B., Silman, I., Sussman, J. L., Gros, P. & Kroon, J. (2001). *Acta Cryst.* D**57**, 566–573.
Weik, M., Schreurs, A. M. M., Leiros, H.-K. S., Zaccai, G., Ravelli, R. B. G. & Gros, P. (2005). *J. Synchrotron Rad.* **12**, 310–317.
Weik, M., Vernede, X., Royant, A. & Bourgeois, D. (2004). *Biophys. J.* **86**, 3176–3185.
Wood, K., Frolich, A., Paciaroni, A., Moulin, M., Hartlein, M., Zaccai, G., Tobias, D. J. & Weik, M. (2008). *J. Am. Chem. Soc.* **130**, 4586–4587.
Wood, K., Plazanet, M., Gabel, F., Kessler, B., Oesterhel, D., Tobias, D. J., Zaccai, G. & Weik, M. (2007). *Proc. Natl Acad. Sci. USA*, **104**, 18049–18054.